TECHNIQUES FOR THE ANALYSIS OF DATA FROM CODED-MASK X-RAY TELESCOPES

G. K. SKINNER, T. J. PONMAN, A. P. HAMMERSLEY, and C. J. EYLES

Department of Space Research, University of Birmingham, Edgbaston, Birmingham, England

(Received 7 April, 1987)

Abstract. Several techniques useful in the analysis of data from coded-mask telescopes are presented. Methods of handling changes in the instrument pointing direction are reviewed and ways of using FFT techniques to do the deconvolution considered. Emphasis is on techniques for optimally-coded systems, but it is shown that the range of systems included in this class can be extended through the new concept of 'partial cycle averaging'.

1. Introduction

Coded-aperture telescopes provide a means of imaging at X-ray energies greater than those which can be focussed by grazing incidence optics but the associated computer analysis can be highly computer-intensive. We consider here some of the tasks which must be accomplished and present some analytical techniques and procedures which have been found to be useful in minimizing the processes involved, including algorithms which provide alternatives to previously published methods. Although we concentrate on methods for optimally-coded systems, we first show that, given appropriate analysis techniques, systems which would otherwise be considered as non-optimum can be included in this category.

2. Optimum Coded Mask Telescopes and Systems which can be Treated as Such

The term 'optimum' is used here to refer to coded mask telescopes in which the design is such that coding errors are non-existent. The only errors are those due to noise – typically counting statistics on the signal and on the detector background. This may be achieved by using cyclic mask designs based on cyclic difference sets and ensuring that the shadow cast on the detector by any source is a whole number of cycles of the mask pattern (Gunson and Polychronopoulos, 1976; henceforth referred to as GP; Fenimore and Cannon, 1978; Proctor *et al.*, 1979). Typically a mask containing $N_x + 1$ by $N_y + 1$ cycles of the pattern and a detector equal in size to N_x by N_y cycles (suitably scaled if the object is not at infinity) are used. An example of such a system with $N_x = N_y = 1$ is shown in Figure 1(a).

If necessary a collimator is used to ensure that flux does not reach the detector from directions such that incomplete shadows would be received. Such a collimator may be combined with the detector (e.g., GP; Proctor *et al.*, 1979) or with the mask (GP) or at an intermediate position (Palmieri, 1974). It must have a full-width-to-zero-response

Astrophysics and Space Science **136** (1987) 337–349.

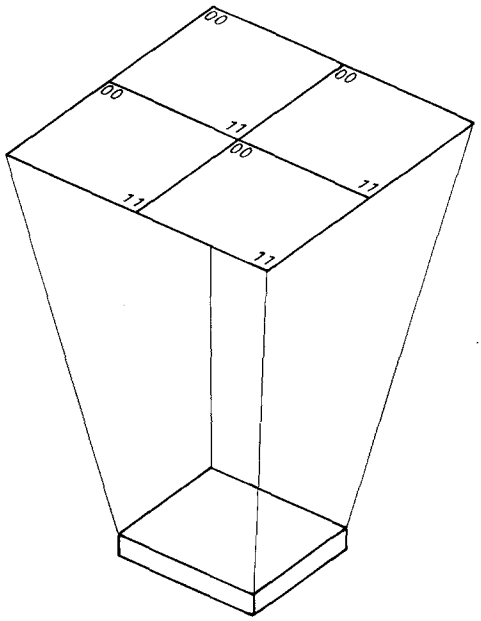

Fig. 1a. An example of an 'optimum' coded-mask telescope. The detector receives one cycle of the shadow of a cyclic mask with two cycles in each direction.

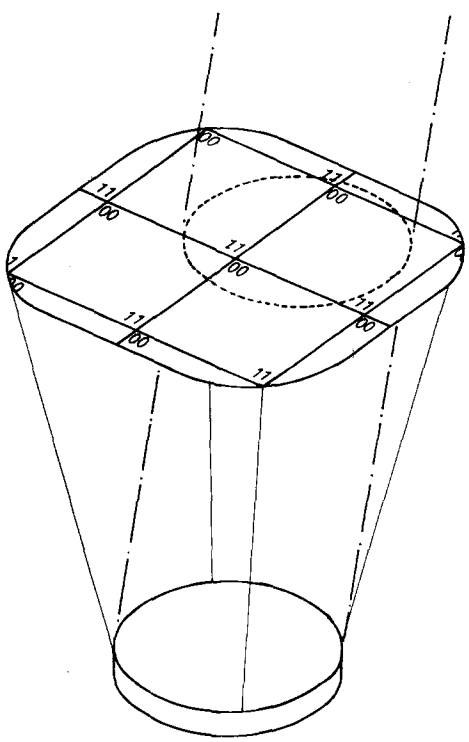

Fig. 1b. A coded-mask telescope with circular detector and a cyclic mask. The arrangement may be treated as an optimum system by using partial cycle averaging. The mask size and shape shown is the minimum for which the shadow of any source in the unambiguous field of view will not be vignetted.

no larger than the angle subtended at the detector by one cycle of the mask or coding errors may arise in the reconstruction.

We will here extend the concept of optimum coded systems to include ones in which the constraint that a whole number of cycles of the mask pattern are recorded is relaxed and we require only that every position in a cycle is recorded at least once and that the data are analysed in such a way that coding errors are absent. Consider as an example the system shown in Figure 1(b) which has a circular detector with a square cyclic mask. In this example the mask cycle is chosen to match the maximum square which can be inscribed in the circle, but the 32% of the sensitive area of the detector in the segments surrounding the central square need not be wasted. The pattern received by any part of the detector within such a segment duplicates that in a position within the square. The two estimates of this signal may be averaged, with a consequent reduction in the uncertainty and, hence, in the noise level in the reconstructed image. We will refer to this technique as 'partial cycle averaging'.

In this example we overcome the problem of properly matching a circular detector to a coded mask, but other circumstances can be envisaged when additional partial shadows are recorded. Provided the data are analysed by folding the recorded data into a single cycle and combining multiple samples, where they occur, by averaging, the imaging properties are unimpaired and we will class such systems as optimum.

The signal to noise ratio obtained in the above example is not quite as good as if it had been possible to utilize the signal from all over the detector with equal weight (some positions in the cyclic shadow are recorded once, others twice). An appropriate figure of merit, proportional to the attainable signal to noise ratio for weak sources, is given by

$$\phi = \int w \, \mathrm{d}m \left(\int w^2 \, \mathrm{d}m \right)^{-0.5},$$

where the integrals are over the detector area and w is the weight given to a pixel as a result of the averaging. For example, where the events in a particular detector pixel will be combined with those from one other which samples the same phase of the mask cycle, $w = \frac{1}{2}$.

As shown in Table I, the performance in the example we have taken is considerably better than if the data outside the square region had been disregarded. Hexagonal-celled masks which utilize most of the area of a circular detector have been proposed (Cook *et al.*, 1984; Haberl, 1984; Fenimore, personal communication). The signal to noise ratio attainable using partial cycle averaging is marginally superior to that obtained by using such a mask (unless of course the hexagonal mask is used *in conjunction with* partial cycle averaging).

3. The Effect of Pointing Errors

The situation will frequently arise where the pointing direction of the telescope is not stable throughout an observation or where data from observations with somewhat

TABLE I

Figures of merit for coded mask telescopes with square and hexagonal masks, with and without partial cycle averaging. The figures are normalised to the value for a hypothetical system in which the entire area of a circular detector is used with equal weight given to all pixels.

Configuration	Relative signal/noise ratio (ϕ)
Hypothetical system using whole of a circular detector with equal weight	1.0
Square mask cycle Data outside square disregarded	$\{2/\pi\}^{0.5} = 0.798$
Hexagonal mask cycle Data outside hexagon disregarded	$\{3\sqrt{3}/2\pi\}^{0.5} = 0.909$
Square mask cycle Using partial cycle averaging	$2\{\pi(3 - \pi/2)\}^{-0.5} = 0.944$
Hexagonal mask cycle Using partial cycle averaging	$\{27/\pi(9\sqrt{3} - 2\pi)\}^{0.5} = 0.961$

different pointing directions are to be merged. In some circumstances the data may be combined in the detector plane into a single amalgamated detector plane image requiring only a single transformation for deconvolution.

This is clearly the case if the telescope motion is a small rotation α_x or α_y about any axis parallel to the mask plane. Such a motion merely translates the shadow cast on the detector by a distance $l\alpha$, where l is the telescope length. If the sensitive area of the detector is physically slightly larger than C mask cycles then the data will still be recorded. More particularly, even if the detector is only the nominal size, the cyclic properties of the system may be utilized. Data which drops off one side of the detector appears on the other! All that is needed is a *cyclic* shift of the detector data.

What is the limit to this procedure? If the shifts become too large then one of several effects may start to become important.

(a) As a result of telescope motion X-rays are accepted, taking the observation as a whole, from a field of view larger than that defined by the collimator. Effectively, the collimator response becomes blurred and wider. Ambiguities can then occur – sources just outside the field of view in one direction can appear, translated by one cycle, just within the opposite border of the field of view. Making the collimator width somewhat smaller than the angle subtended by one mask cycle can alleviate this problem.

(b) The blurring of the collimator response described above will have to be taken into account even for the central parts of the image if intensities are to be determined accurately. This will normally involve some simplifications and approximations and these may become intolerable if the cyclic shifts become too large.

(c) For wide field systems projection effects become important. For a photon from a source at an angle φ off-axis in the direction of the telescope movement the correction $l\alpha$ should strictly be $l\alpha \sec^2 \varphi$. Of course φ is not known for individual photons, so any

correction made is only approximate and the application of large corrections can lead to errors.

We have so far only considered rotations of the telescope about axes parallel to the mask. A rotation α_z about an axis normal to the mask is less serious if small, as the maximum amount by which a feature in the shadow is displaced with respect to the detector is $l\alpha_z \tan \varphi$ where φ is again the off-axis angle of the source causing the shadow, which is necessarily smaller than the size of the field of view. If, however, the motion cannot be ignored (which occurs when shifts near the edge of the field become comparable with the dimensions of one pixel) then α_z errors are more difficult to handle because φ is different for photons from different sources. The only possibility is to reconstruct images for periods during which the effect is negligible for the sources at greatest φ and then to add the resultant images. We return to methods for adding offset images in Section 5.

4. The Deconvolution Process

4.1. The problem to be solved

Consider an 'optimum' coded-mask telescope (in the sense used above) with m by n elements. We ignore for the present the effect of any collimator. The best estimate of the source flux distribution is a linear function of the 2-d (two-dimensional) cyclic cross-correlation function between the array (D) of intensities observed in the detector plane an an array (M) representing the mask pattern, is

$$S(x, y) = P + Q\left[\sum_{i=0}^{m-1}\sum_{j=0}^{n-1} D(i, j)M((x - i)_{\mathrm{mod}\, m}, (y - j)_{\mathrm{mod}\, n})\right]. \qquad (1)$$

Although strictly this equation does not apply to non-optimum systems it is often a useful approximation.

Here m and n are the dimensions of the array into which the detector data are binned. They do not have to be equal to the number of elements in a mask cycle – we may choose to make the summation over sub-pixels, smaller in each dimension than the mask pixels by integer factors. M will then have repeated values. Fenimore and Cannon (1981) have called this case fine-sampling and a simple variation of it, in which the $+1s$ in M are not repeated, delta-decoding. We use the term sub-pixelling here to refer to either of these methods, but we note that the latter is more generally useful because the equivalent 'fine-sampled' image can be obtained from a 'delta-decoded' one with a simple block filtering operation.

The values of P and Q depend on the definition of flux used, on the form chosen for M and the way that background levels are to be handled. It is convenient to choose flux units such that an image value of S_x means that there were S_x photons detected from a source in that pixel during the time for which the data were accumulated. If M has the values ± 1 and we wish to use 'balanced decoding', as defined by Fenimore and Cannon (1978), such that the flat sides lobes of the point source response function are

at the zero level then the required values are

$$P = \frac{N(1-2t)+1}{2N(1-t)}\,\Sigma D\,, \qquad Q = \frac{N-1}{2N(1-t)}\,,$$

where t is the fraction of transparent elements in the mask pattern (the fraction of $+1$ elements in M), ΣD is the total signal in the detector (after any background has been subtracted) and $N = nm$.

Balanced decoding in this sense has little advantage in practice as the circumstances in which coded mask telescopes offer an advantage are those in which detector background dominates over the signal. Generally the background counting rate will not be sufficiently accurately known for it to be precisely subtracted and in these circumstances the above values of P, Q lead to a bias level in the image which is equal to B, where B is the mean (residual) background rate per detector pixel.

An alternative which is particularly appropriate where one is searching for a small number of weak sources is to arrange that the image has a known mean level – conveniently a mean of zero. This can be achieved by using

$$P = \frac{(1-2t)}{2(1-t)}\,\Sigma D \quad \text{and} \quad Q = \frac{1}{2(1-t)}\,.$$

An image obtained in this way obviously contains no information about a very extended source having the same intensity in every pixel. The problem is inevitable because we cannot deduce independent measurements of the mn image pixels and the detector background, a total of $mn + 1$ parameters, from the mn measurements of the fluxes in the detector pixels.

We note that this does not mean that data from coded mask telescopes contain no information about the diffuse X-ray background as we have so far ignored the effect of any collimator which is used to limit the field of view. Typically such a collimator will modulate the diffuse background, imposing a pyramidal form on it in the intensity units used here and, given sufficient sensitivity, allowing information about it to be derived.

4.2. Performing the deconvolution

If the mask pattern is one based on Singer cyclic difference sets (i.e., on base-2 m-sequences) the cross-correlation is most easily performed using Hadamard transform techniques (Skinner, 1980; Gunson and Skinner, 1979; Fenimore, 1983). For other mask patterns the best procedure is not so obvious. We will discuss in a future paper fast techniques which can be used with mask patterns based on twin-prime cyclic difference sets and restrict ourselves here to considering the optimum strategy for using Fourier transform techniques, which are not restricted to any particular pattern.

A cross-correlation such as (1) can be performed by a Discrete Fourier Transform (DFT)

$$S = P + Q(\mathrm{DFT}^{-1}(\mathrm{DFT}(D)\mathrm{DFT}(M)))\,. \tag{2}$$

The Fast Fourier Transform (FFT) algorithm can be used to perform the transforms, but in a typical case doing this in a straightforward way leads to a very inefficient implementation. Often m, n will be either prime numbers (for mask patterns based on twin-prime cyclic difference sets) or of the form $2^p - 1$, $2^p + 1$ (for those based on base 2 m-sequences). The most efficient and common 2-d FFT algorithm requires that each dimension of the array transformed is of the form 2^N. To use this involves either extending the arrays or re-sampling.

Extending the D array in each direction by repeating it cyclically and the M array by padding with zeroes, such that each dimension is at least twice the original one and is equal to a power of two as shown in Figure 2(a), achieves the desired effect. The size

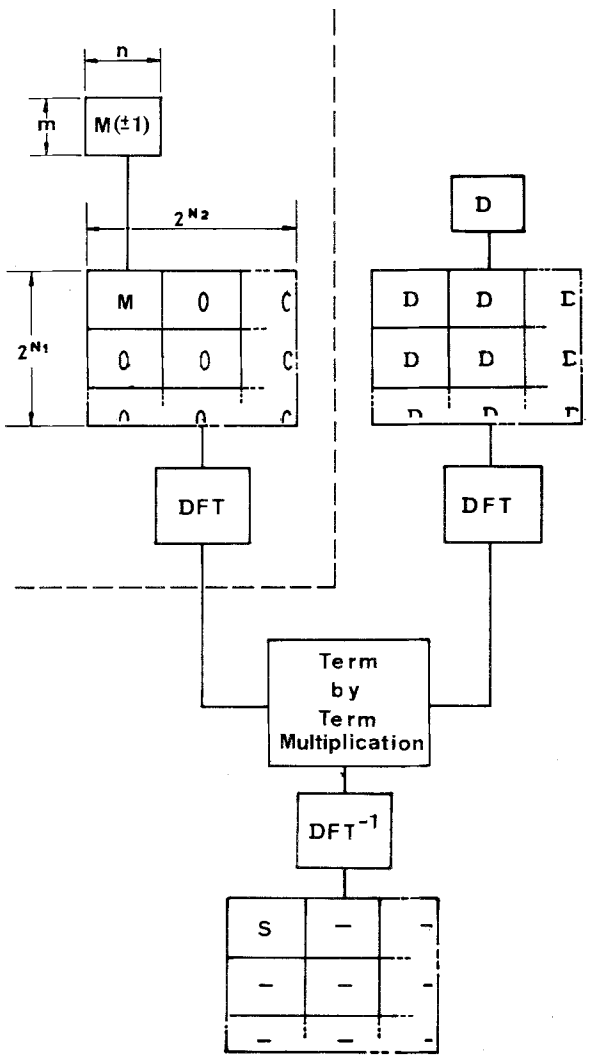

Fig. 2a. Use of a 2-d FFT to cross-correlate two arrays with arbitrary dimensions. One array is repeated cyclically and the other padded with zeroes to obtain arrays of dimension 2^{N_1} by 2^{N_2} where $2^{N_1} > 2m$ and $2^{N_2} > 2n$.

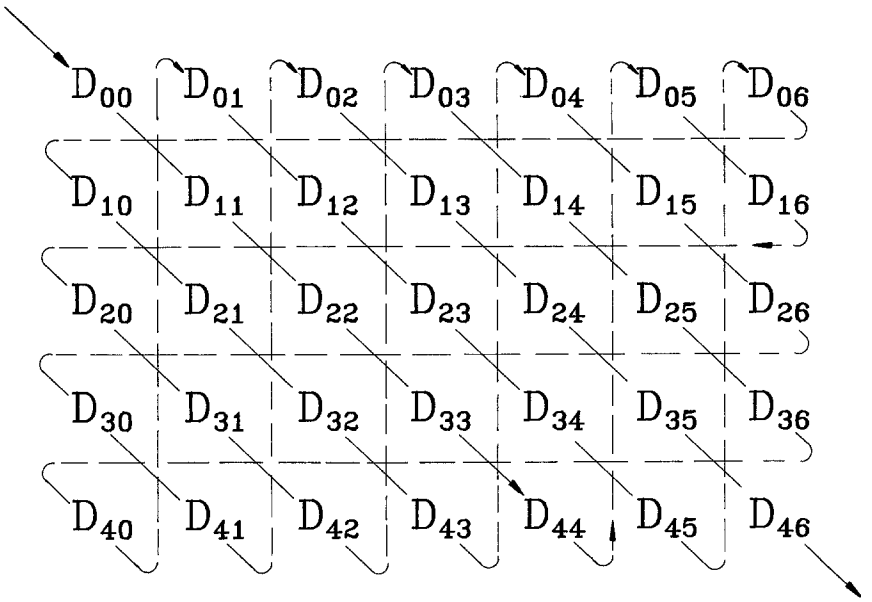

Fig. 2b. Mapping a two-dimensional array onto a one-dimensional one so that a 1-d FFT can be used with padding by less than a factor of 2.

of the transforms to be performed is, however, greatly increased. For example, in the case where $m = 2^p - 1$, $n = 2^p + 1$ the number of elements in the arrays to be transformed goes up by a factor ~ 8. This scheme is similar to that proposed by Fenimore and Cannon (1981), although they suggested a larger extension of the arrays.

Re-sampling can reduce the amount of processing but formally destroys the ideal mask properties (although Fenimore and Cannon (1981) show that the additional noise may be small) and may introduce systematic biases in source positions.

For arrays where m and n have no common factors there is an alternative approach in which we map the arrays D, M, S onto 1-d arrays

$$D'(k) = D(i, j), \qquad M'(k) = M(i, j), \qquad S'(k) = S(i, j);$$

where

$$i = (k)_{\mathrm{mod}\, m} \quad \text{and} \quad j = (k)_{\mathrm{mod}\, n},$$

(see, for example, Figure 2(b)). If m and n are mutually prime, the Chinese remainder theorem ensures a one-to-one correspondence between the elements of 1-d and 2-d arrays. This mapping has the property that

$$k(i + \Delta i, j + \Delta j) = k(i, j) + k(\Delta i, \Delta j);$$

with the result that

$$D * M = K^{-1}(K(D) * K(M)),$$

where i, j, k are defined modulo m, n, mn and where * is the convolution operator and K, K^{-1} are operators describing the forward and reverse mapping. Thus we may replace the 2-dimensional cross-correlation by a 1-dimensional one.

The extension of the arrays to allow a base 2 FFT to be used is now required only in one dimension. In the most unfavourable case this requires less than a factor of 4 increase in the number of elements; for the $m = 2^p - 1$, $n = 2^p + 1$ case the factor is

$$2^{2p+1}/(2^{2p} - 1) \sim 2 .$$

By way of example we show in Table II the array sizes and some processing times for a 255 by 257 element array using this technique and employing a 2-d FFT. Despite the overheads associated with the mapping and unmapping, the 1-d approach is faster by nearly a factor of four.

TABLE II

Array sizes and processing times for a 255 by 257 element deconvolution using the method of Section 4 and using a straightforward padded 2-d FFT. The times are measured cpu seconds on a MicroVax II with 9 Mbites of memory. In each case deconvolution is by cross-correlation with a pattern for which the Fourier transform is precalculated.

Method	Array cross-correlated	Size of FFT	Overall execution time (s)
1-d	1 by 65535	1 by 131072	51.6
2-d	255 by 257	512 by 1024	192.4

Provided that no sub-pixelling is used the requirement that m and n have no common factors is met by arrays corresponding to both of the types of mask pattern mentioned above. If sub-pixelling is used the property will be lost unless the numbers f_x, f_y of sub-pixels per pixel in the two dimensions are different and are selected carefully. The delta-decoding transform can, however, still be accomplished by separating the 2-d arrays into $f_x f_y$ interleaved component arrays and performing separate transforms of size $\sim 2mn/f_x f_y$ on each component, a similar size computation. This is analogous to the technique used to achieve sub-pixelling when Hadamard transforms are employed, which has been described in detail by Fenimore and Weston (1981).

5. Combining Data from Different Pointing Directions

Combining images when there has been appreciable telescope movement is a comparatively straightforward task if the instrument has a small field of view. One of the advantages of coded-mask telescopes is, however, that a wide field of view can be obtained and it will frequently be the case that small-angle approximations cannot be made. Efficient handling of the computation involved is particularly important as the effect is most likely to be important when there are many pixels.

The result of a single reconstruction operation is a map representing the intensities in sky pixels whose directions are such that radiation falling on a reference point in the

detector, for example the centre, will have passed through different elements of the mask. Thus the image is regularly sampled on a regular grid in a gnomonic projection of the sky, the pole of the projection being the pointing direction. When we come to combine data from different observations the images will, in general, be grids in gnomonic projections with different poles and with different orientations. If we adopt one such grid as a standard onto which we will add data from the other observations, then we have the problem of finding the position in the base grid corresponding to each point in each subsidiary grid.

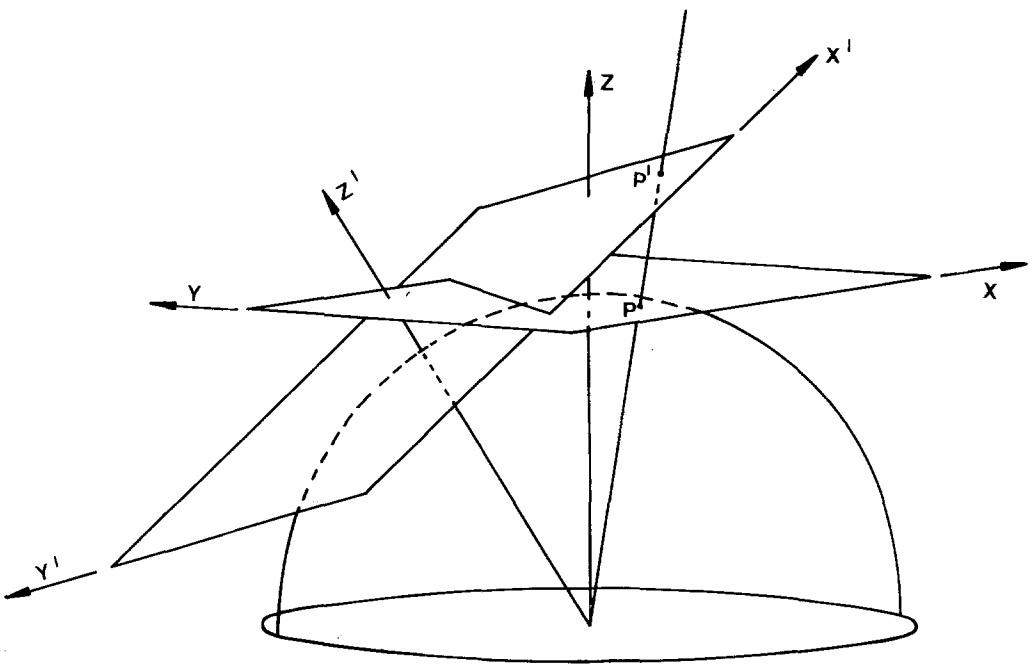

Fig. 3. The projective geometry for transform between two pointing directions. The arrows show the only direction of the axes; the origin is at the centre of the celestial sphere.

As can be seen from Figure 3, this is a simple problem in projective geometry. Computationally it is efficiently handled in the following way. The pixel P' in the subsidiary plane can be represented by Cartesian coordinates $(x', y', 1)$ in the coordinate system shown. We have chosen a scale such that z is unity for points in the tangent plane. Expressed in a similar coordinate system in the base frame, P' will have coordinates (x, y, z), where z is no longer unity.

The transformation from (x, y, z) to (x', y', z') is described by the rotation of the telescope from the base frame to the subsidiary frame. This can be described by Euler angles α_z, α_x, α_y (these are the rotations about the z-axis, the (new) x-axis and the (new) y-axis necessary to move from the base pointing direction to the subsidiary one). The sky direction corresponding to P' will be represented in the base frame by a point P whose coordinates are obtained by applying the inverse rotation matrix to those of P

matrix to those of P and renormalising: i.e.,

$$\begin{bmatrix} x \\ y \\ z \end{bmatrix} = (R^{-1}) \begin{bmatrix} x' \\ y' \\ z' \end{bmatrix},$$

where

$$R^{-1} = \begin{Bmatrix} \cos\alpha_y \cos\alpha_z - \sin\alpha_x \sin\alpha_y \sin\alpha_z & -\cos\alpha_x \sin\alpha_z & \sin\alpha_y \cos\alpha_z + \sin\alpha_x \cos\alpha_y \sin\alpha_z \\ \cos\alpha_y \sin\alpha_z + \sin\alpha_x \sin\alpha_y \cos\alpha_z & \cos\alpha_x \cos\alpha_z & \sin\alpha_y \sin\alpha_z - \sin\alpha_x \cos\alpha_y \cos\alpha_z \\ -\cos\alpha_x \sin\alpha_y & \sin\alpha_x & \cos\alpha_x \cos\alpha_y \end{Bmatrix},$$

$$x_0 = x/z\,, \qquad y_0 = y/z\,.$$

Clearly R^{-1} and, hence, the trigonometrical functions, need be computed only once for each subsidiary image and further savings can be made if the x', y' grid is rectangular.

When corresponding points in the two images have been identified the incident flux estimates, corrected for the collimator response and observation time in each case, can be combined. It is important to form a weighted mean as the uncertainties in the two measurements can be very different, particularly if the pixel is close to the edge of the collimator response in one case.

6. Conclusions

As an example of the application of the techniques described in Sections 3 and 5 we show in Figure 4 a part of an image of the Crab nebula X-ray source obtained with the Spacelab 2 coded-mask telescope (Willmore *et al.*, 1984). In Figure 4(a) no corrections have been applied for telescope movement during the observation. Although the pointing of the telescope z-axis was relatively stable, the fact that only a two-axis gimbal-mount was used resulted in an appreciable rotation about the pointing axis. Separate images were then obtained from 38 subsets of the data, correcting photon positions for x and y rotations within each. The images were combined using the method described in Section 5. The resulting peak (4b) is consistent with the nominal resolution of the telescope (3.0 arc min full width at half maximum (FWHM); 6.0 arc min to zero response), slightly broadened by the finite size of the X-ray emitting region (42 arc sec FWHM, Wolff, 1975) and by the detector spatial resolution (equivalent to ~ 40 arc sec FWHM).

We have presented techniques useful in all the stages of coded-mask telescope data analysis. In forming arrays recording the mask shadow we have shown how the concept of an optimum coded-mask telescope may be extended. In the deconvolution process,

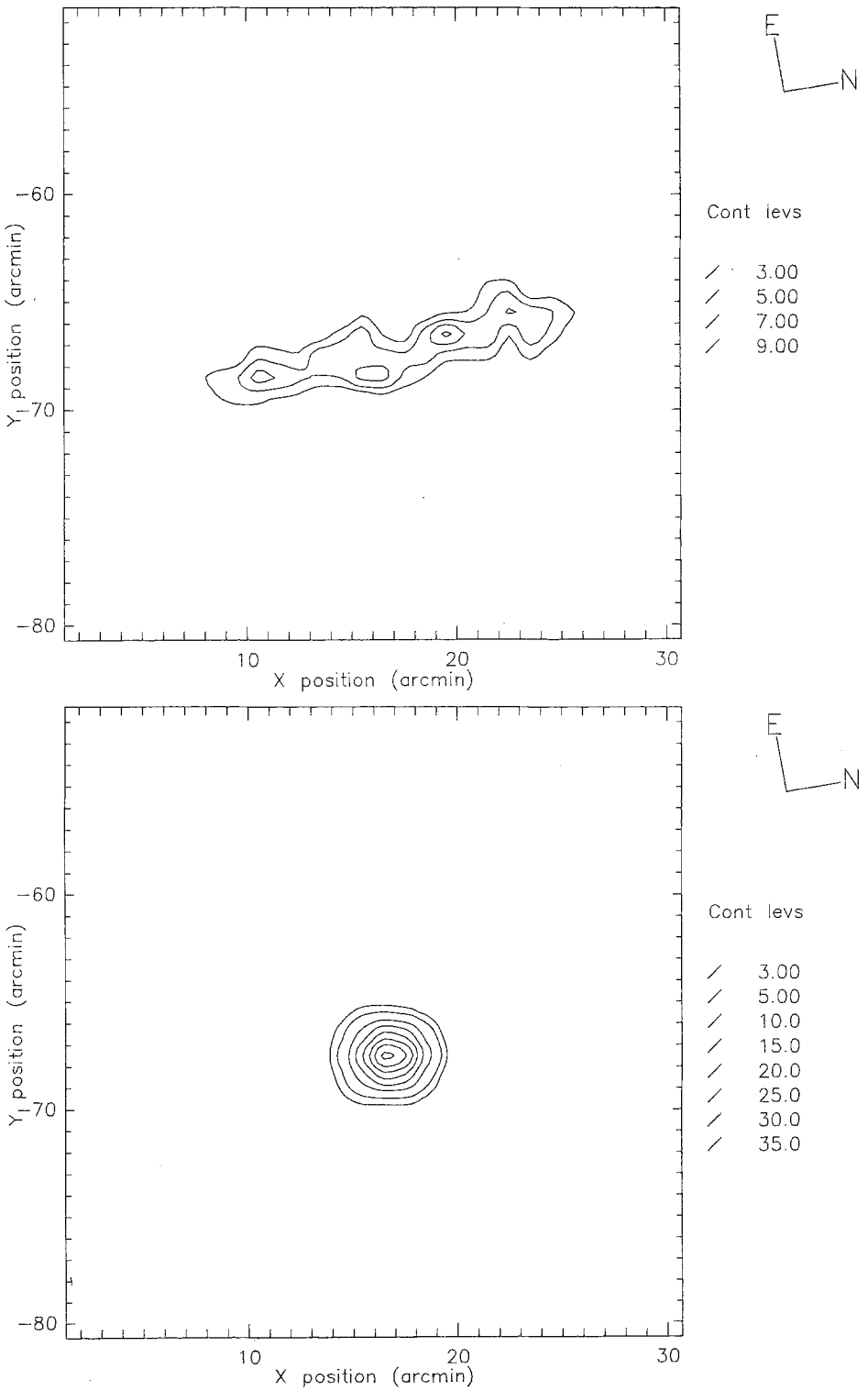

Fig. 4. An X-ray image of the Crab nebula (a) without correction for pointing direction changes, (b) corrected using the techniques of Sections 2 and 5.

the correct procedures to use in order to handle bias levels due to detector background in the best way have been discussed and a method of efficiently performing the deconvolution using a one-dimensional FFT was given. Lastly, we have discussed the procedures necessary to cope with telescope movement-correcting photon positions in the detector plane where this is possible and combining shifted images where it is not.

Acknowledgements

Much of the work described here resulted from experience in analysing data from the coded-mask X-ray telescope flown on the Spacelab 2 mission. We are grateful to SERC and to NASA for support of that project. We are indebted to the many colleagues involved in the Spacelab 2 mission and in subsequent data analysis work. The Spacelab 2 data analysis is being conducted using the facilities of the Starlink network, supported by the SERC.

References

Cook, W. R., Finger, M., Prince, T. A., and Stone, E. C.: 1984, *IEEE Trans. on Nucl. Sci.*, NS-31, 771.

Fenimore, E. E.: 1983, *Appl. Optics* **22**, 826.

Fenimore, E. E. and Cannon, T. M.: 1978, *Appl. Optics* **17**, 337.

Fenimore, E. E. and Cannon, T. M.: 1981, *Appl. Optics* **20**, 1858.

Fenimore, E. E. and Weston, G. S.: 1981, *Appl. Optics* **20**, 3058.

Gunson, J. and Polychronopoulos, B.: 1976, *Monthly Notices Roy. Astron. Soc.* **177**, 485.

Gunson, J. and Skinner, G. K.: 1979, 'A Fast Convolution Transform for *m*-Sequences', University of Birmingham, unpublished report.

Haberl, F.: 1984, MPE Report 182.

Wolff, R. S., Kestenbaum, H. L., Ku, W., and Novick, R.: 1975, *Astrophys. J.* **202**, L15.

Palmieri, T. M.: 1974, *Astrophys. Space Sci.* **20**, 431.

Proctor, R. J., Skinner, G. K., and Willmore, A. P.: 1979, *Monthly Notices Roy. Astron. Soc.* **187**, 633.

Skinner, G. K.: 1980, *J. Brit. Interplanetary Soc.* **33**, 333.

Willmore, A. P., Skinner, G. K., Eyles, C. J., and Ramsey, B.: 1984, *Nucl. Instr. Methods Phys. Res.* **221**, 284.